NANO LETTERS

pubs.acs.org/NanoLett Letter

From Sodium–Oxygen to Sodium–Air Battery: Enabled by Sodium Peroxide Dihydrate

Xuanxuan Bi, Rongyue Wang, Yifei Yuan, Dongzhou Zhang, Tao Zhang, Lu Ma, Tianpin Wu, Reza Shahbazian-Yassar, Khalil Amine,* and Jun Lu*

Cite This: *Nano Lett.* 2020, 20, 4681–4686 Read Online

ACCESS | Metrics & More | Article Recommendations | Supporting Information

ABSTRACT: Metal–air batteries have attracted extensive research interests due to their high theoretical energy density. However, most of the previous studies were limited by applying pure oxygen in the cathode, sacrificing the gravimetric and volumetric energy density. Here, we develop a real sodium–"air" battery, in which the rechargeability of the battery relies on the reversible reaction of the formation of sodium peroxide dihydrate ($Na_2O_2{\cdot}2H_2O$). After an oxygen evolution reaction catalyst is applied, the charge overpotential is largely reduced to achieve a high energy efficiency. The sodium–air batteries deliver high areal capacity of 4.2 mAh·cm^{-2} and have a decent cycle life of 100 cycles. The oxygen crossover effect is largely suppressed by replacing the oxygen with air, whereas the dense solid electrolyte interphase formed on the sodium anode further prolongs the cycle life.

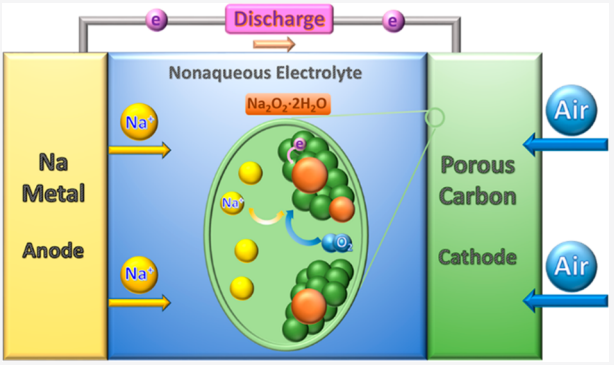

KEYWORDS: *Sodium–air batteries, Nanocomposite PtNi, Sodium–oxygen batteries, Sodium peroxide dihydrate*

INTRODUCTION

Metal–air batteries have acquired extensive research interests in the past decade owing to their high theoretical energy density and high capacity.[1−3] Nevertheless, most studies rely on pure oxygen gas as the active medium instead of air.[4,5] With Li_2O_2 as an ideal product, aprotic lithium–oxygen (Li–O_2) batteries have a theoretical energy density of ∼3500 Wh·kg^{-1}, but the inclusion of oxygen would largely decrease the number due to the addition of oxygen facility.[6,7] Air contains N_2, O_2, H_2, CO_2, Ar, and humidity (H_2O), in which most species, except Ar, react with lithium metal and the product, Li_2O_2.[8−10] Replacing oxygen with air could be extremely challenging at the current stage. A similar scenario is observed in sodium–oxygen (Na–O_2) batteries where the product NaO_2 is highly reactive.[11,12] Not only would it react with CO_2 and water,[13−15] but its stability is problematic under an ambient atmosphere.[16−18] NaO_2 could also react with the electrolyte to form Na_2CO_3,[9] not to mention the possible shuttle effect caused by the dissolution of NaO_2.[19,20] Therefore, even resting the cell could be harmful as NaO_2 may disappear before the next cycle.

Given the difficulties of using air in the cathode, limited studies have been performed in a real air environment. Asadi et al. attempted to assemble a lithium–air (Li–air) battery in an air-like atmosphere and achieved a long cycle life with Li_2O_2 as the discharge product.[21] Although they show that Li_2O_2 is not likely reacting with a low concentration of CO_2 and H_2O, the long lasting stability of Li_2O_2 in air is highly questionable. On the other hand, there has been very limited studies on a rechargeable Na–air battery because the increased water vapor in air leads to the irreversible formation of $NaOH{\cdot}H_2O$ and Na_2CO_3.[22] Obviously, obtaining a stable and rechargeable product in air is the key to achieve a rechargeable "air" battery.

Different from the Li–air battery, where Li_2O_2 is a typical discharge product that is unfortunately hard to survive in air, a Na–air battery has shown more versatility on the discharge products, including sodium peroxide dihydrate ($Na_2O_2{\cdot}2H_2O$), in addition to the well-known NaO_2.[23] Theoretically, $Na_2O_2{\cdot}2H_2O$ should be more tolerant to H_2O and CO_2[14,24,25] and thus the air. More intriguingly, the formation of $Na_2O_2{\cdot}2H_2O$ in a Na–air cell certainly requires humidity (H_2O), making it a potential candidate that could be stabilized in air but has yet to be explored. The absence of investigations in air environment are due to not only the lack of stable product but also the instability of the anode. Oxygen crossover is well recognized as a detrimental effect to the alkali metal anode, resulting in the formation of many oxidative side products.[26,27] However, owing to less oxygen partial pressure in air, the effect

Received: April 17, 2020
Revised: May 18, 2020
Published: May 19, 2020

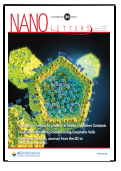

https://dx.doi.org/10.1021/acs.nanolett.0c01670
Nano Lett. 2020, 20, 4681–4686

of oxygen crossover could be largely suppressed in the anode. Based on these observations, sodium−air batteries show great potential to be applied in air.

Here, we successfully achieve a rechargeable sodium−air battery exhibiting stable voltage profiles and long cycle life of 80 cycles. To reduce the high charge overpotential, we further employ a catalyst to facilitate the oxygen evolution reaction and prolong the cycle life to over 100 cycles. $Na_2O_2{\cdot}2H_2O$ is confirmed to be the main discharge product. More importantly, we prove the reversibility of the formation and decomposition of $Na_2O_2{\cdot}2H_2O$ through a two-electron transfer reaction: $2Na + O_2 + 2H_2O \leftrightarrow Na_2O_2{\cdot}2H_2O$. A stable solid electrolyte interphase (SEI) was formed on the surface of Na metal, which allowed the anode to survive after long cycles. We believe this study will highlight the importance for the development of real sodium−"air" batteries and pave a way for the practical application of sodium−air batteries.

RESULTS AND DISCUSSION

The sodium−air battery is assembled by stacking a sodium metal anode, a glass fiber (Na_2SiO_3) separator soaked with 1 M Na triflate in DEGDME, and carbon fiber paper[28−31] in a homemade stainless steel cell. Air flows into the cell with the pressure slightly over 1 atm. The percentage of each gas in air is listed in Table S1, measured by a mass spectrometer. Air contains approximately 77.03% N_2, 19.47% O_2, 0.60% H_2, 0.56% CO_2, 1.06% Ar, 1.27% H_2O, and 0.01% other gases, averaged by three tests with errors of ±0.5%. To ensure the stability of the electrolyte in air, cyclic voltammetry was performed to test the electrochemical window of the dry electrolyte and the electrolyte with 4000 ppm water, shown in Figure S1. The addition of water does not create severe electrolyte decomposition. In this case, we assembled the Na−air battery and performed galvanostatic tests. Figure 1a shows the voltage profiles of the sodium−air cell with air as the active medium in the cathode. During the first cycle, the discharge voltage is around 2.2 V, whereas the charging process shows three plateaus, located at 2.4, 3.2, and 4.0 V. The voltage profiles are typical for $Na_2O_2{\cdot}2H_2O$ formation and decomposition.[32] From our previous in situ X-ray diffraction (XRD) studies, we observe the discharge is only related to $Na_2O_2{\cdot}2H_2O$ formation.[24] The charging process is related to $Na_2O_2{\cdot}2H_2O$ decomposition, NaOH formation at around 3.2 V, and other side product formation at 4.0 V. For the following cycles, only one plateau is observed during the charge (~4.0 V). It is very likely that the defects on the carbon fiber paper react with the electrolyte and are covered by the side products at the first cycle. The following cycle is not affected by the defects, resulting in one plateau. In addition, the formation of the side products during the first cycle may contribute to the elevated resistance of the air electrode, thus increasing the charging voltage. The formation of the side products during the first cycle may contribute to the elevated resistance of the air electrode, thus increasing the charging voltage. Although the charge voltage is high, this sodium−air cell still has a cycle life of 80 cycles and the cell voltage has almost no changes during the following cycles, indicating a relatively stable cell environment. This finding confirms that, even replacing the oxygen by air, the cell undergoes a reversible reaction without much influence of other active species in air.

The morphology and the distribution of discharge product were investigated by scanning electron microscopy (SEM) and energy-dispersive X-ray spectroscopy (EDS) mapping. The

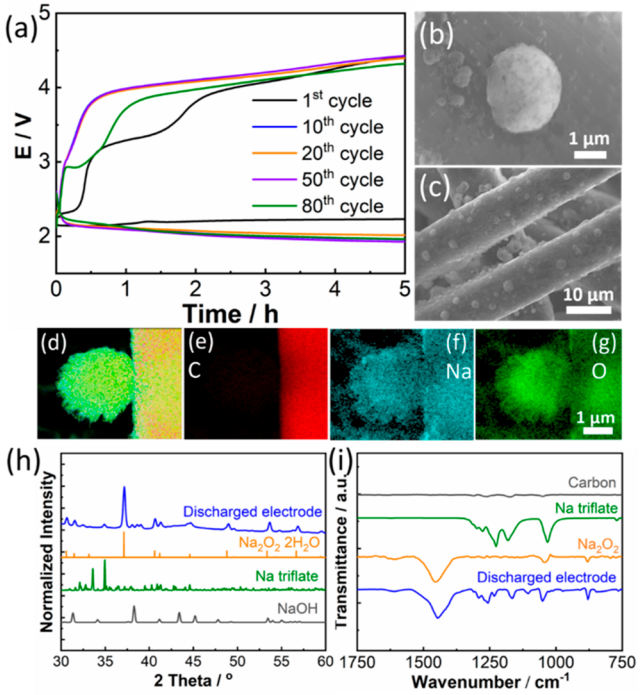

Figure 1. (a) Voltage profiles and cycle life of the sodium−air batteries with air atmosphere as the cathodic source. The current density is 0.05 $mA{\cdot}cm^{-2}$. Scanning electron microscopy images (b,c) and energy-dispersive X-ray spectroscopy mappings (d) of C (e), Na (f), and O (g) of the discharged electrode in the sodium−air battery. (h) X-ray diffraction of the discharged electrode, standard $Na_2O_2{\cdot}2H_2O$ diffractions (JCPDS ref # 15-0064), Na triflate, and NaOH (JCPDS ref # 35-1009). (i) Fourier transform infrared spectrum of the discharged electrode, pristine carbon paper, Na triflate salt, and commercial Na_2O_2. The discharged electrode was obtained in the sodium−air battery discharged to a capacity of 1 $mAh{\cdot}cm^{-2}$.

sodium−air battery was discharged for 20 h at a current density of 0.05 $mA{\cdot}cm^{-2}$, with an areal capacity of 1 $mAh{\cdot}cm^{-2}$. Figure 1b,c shows the SEM images of the discharge product with different magnifications. The discharge product has a spherical structure with a diameter of 2 μm and evenly deposits on the surface of carbon fibers. The EDS mapping shows the distribution of the elements, C, Na, and O, in a localized particle (Figure 1d−g). At a closer look in Figure 1d, the particle has an inner core with a fluffy outer surface. The particles comprise Na and O, indicating the formation of a Na−O-based product.

To identify the crystalline structure and the composition of the discharge products, XRD and Fourier transform infrared spectroscopy (FTIR) were carried out. Figure 1h shows the XRD patterns of the discharged electrode, $Na_2O_2{\cdot}2H_2O$ (JCPDS ref # 15-0064), Na triflate salt, and NaOH (JCPDS ref # 35-1009). The diffractions of the discharge product match well with the standard $Na_2O_2{\cdot}2H_2O$ peaks, confirming that it is the main discharge product. We also observe small signals of the sodium triflate at 35.0° and NaOH at 38.3°. The formation of NaOH is likely due to the decomposition of the electrolyte or the parasitic reaction from the humidity. Figure 1i shows the FTIR spectra of the discharged electrode with the references, pristine carbon paper, Na triflate salt, and commercial Na_2O_2. The discharged electrode shows the characteristic peaks of Na_2O_2, located at 879 and 1447 cm^{-1},[33,34] indicating the presence of Na_2O_2-based species in

https://dx.doi.org/10.1021/acs.nanolett.0c01670
Nano Lett. 2020, 20, 4681−4686

the discharge product. To further reveal that the electrochemical reaction occurred in the sodium−air battery, we performed a galvanostatic intermittent titration technique (GITT), shown in Figure S2. The sodium−air battery first discharged for 20 min and stayed for 3 h to reach the equilibrium. The equilibrium potential is observed to be 2.32 V, which is consistent with the previously reported reaction: $2Na + O_2 \rightarrow Na_2O_2$, $E^0 = 2.33$ V.[35]

As the charging overpotential is high in sodium−air batteries (close to 2 V), we considered using catalysts to reduce the overpotential in order to obtain a higher energy efficiency. Multiple catalysts have been probed, such as single noble metal catalysts including Pt nanoparticles, alloy catalysts including PtNi nanoparticles, metal oxide catalysts including NiO and Co_3O_4,[36,37] where PtNi nanoparticles show the best catalytic performance, compared in Figure S3. Here, we employ the PtNi nanoparticles (NPs) as the catalyst. They were fabricated by a wet chemistry method (experimental section in Supporting Information). Figure 2a shows a uniform

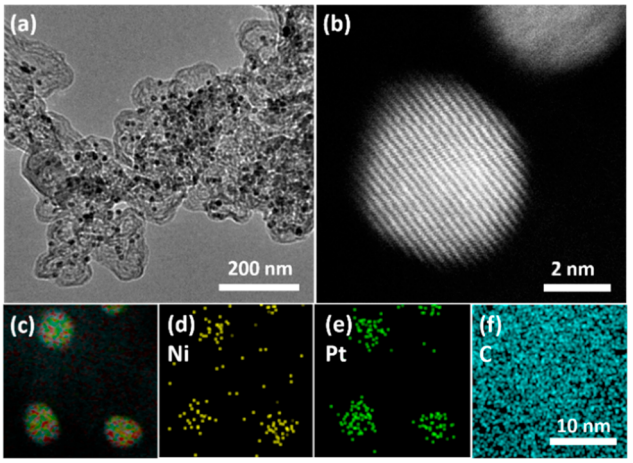

Figure 2. (a) TEM image and (b) HAADF-STEM of PtNi/C catalysts. (c) TEM image and EDS mappings of (d) Ni, (e) Pt, and (f) C. The scale bar of (c−e) is the same as that in (f).

distribution of PtNi NPs on TKK carbon. The high-angle annular dark-field scanning transmission electron microscopy (HAADF-STEM) image[38] in Figure 2b shows a crystallized PtNi nanoparticle with a particle size of 4 nm, and Figure 2c−f displays the distribution of Pt and Ni in the localized particle. In Figure S4, the diffractions of PtNi NPs shift to a higher angle compared to the standard diffraction of Pt, implying the shortening of the lattice plane and the formation of the PtNi alloy. The valence state of Pt and Ni in the alloy was further investigated by X-ray absorption spectroscopy. The oxidation state of Pt in PtNi matches closely with that of the reference Pt, whereas the Ni has a white line intensity higher than that of the Ni foil, indicating the oxidation of Ni on the surface (Figure S5).[39]

After the PtNi/C catalyst was applied in the sodium−air battery, the charge voltage was largely reduced, resulting in a much-improved energy efficiency. As shown in Figure 3a, the cell with PtNi/C has a charging voltage of 2.7 V at the first cycle, and with the increase of the cycle number, the charge potential keeps increasing but still maintains below 3.7 V at the end of the 100th cycle. The increased charge overpotential is likely due to the accumulation of side products on the air electrode to cover the active sites of the catalyst. Figure 3b

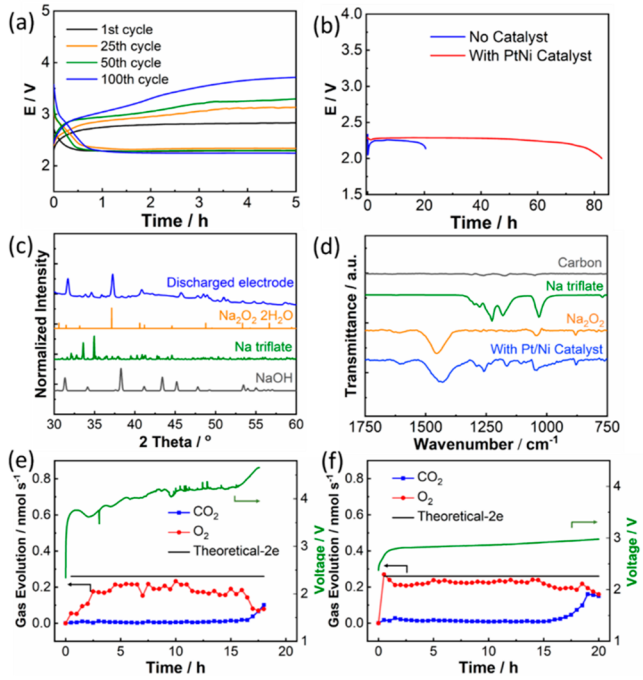

Figure 3. (a) Voltage profiles and cycle life of sodium−air batteries with the PtNi/C catalyst. (b) Comparison of the deep discharge profiles of sodium−air batteries without catalyst and with PtNi/C catalyst. (c) XRD and (d) FTIR of the discharged electrode (blue lines) in the sodium−air battery with the PtNi/C catalyst. The discharged electrode is obtained in the sodium−air battery discharged to a capacity of 1 mAh·cm^{-2}. Differential electrochemical mass spectrometry (DEMS) and charging profiles of the sodium−air batteries (e) without catalysts and (f) with a PtNi/C catalyst. The current density is 0.05 mA·cm^{-2} for all cells. For DEMS measurements, the cells first discharge for 20 h and then charge in DEMS.

shows the deep discharge profiles of the cell with the PtNi/C catalyst and without a catalyst. The cell without the catalyst only delivers a capacity of 1.4 mAh·cm^{-2}, whereas the capacity increases to 4.2 mAh·cm^{-2} with the catalyst, which benefits from the increased active sites from the catalyst. From Figure 3b, we observe a slight increase of the discharge voltage when the catalyst is employed, which is likely because the active sites provided by the catalyst facilitate the kinetics during the oxygen reduction reaction. The discharge product is confirmed by XRD and FTIR. Figure 3c shows that the major patterns of the discharged electrode are related to $Na_2O_2{\cdot}2H_2O$, evidencing that it is the main discharge product when the catalyst is applied. The discharged electrode also shows the signals of Na triflate and a sign of NaOH, which could probably be due to the decomposition of the electrolyte. FTIR (Figure 3d) further proves the formation of NaOH-based product. The findings confirm that the PtNi/C catalyst effectively reduces the charging voltage and enhances the discharge capacity of the sodium−air batteries.

The rechargeability of the sodium−air batteries is investigated by SEM, XRD, and differential electrochemical mass spectroscopy (DEMS). Figure S6 shows the SEM images of the discharged electrode and charged electrode without the catalyst. After the charging process, we no longer observed the particle-like product, indicating the removal of the discharge product. XRD in Figure S7 further demonstrates the diffractions of the charged electrodes in sodium−air batteries without and with the PtNi/C catalyst. In both scenarios, the

https://dx.doi.org/10.1021/acs.nanolett.0c01670
Nano Lett. 2020, 20, 4681−4686

discharge product, $Na_2O_2·2H_2O$, was removed from the electrode after the charging process, indicating a reversible electrochemical reaction. Previous study also shows that $Na_2O_2·2H_2O$ could reversibly decompose during charging in O_2 at a higher charge voltage.[34]

To further reveal the reversibility, we performed DEMS measurement on both cells, shown in Figure 3e. The two cells were tested during the charging process after being discharged for 20 h. The gas sample, which was generated from the electrochemical cell, was injected into the mass spectrometer every 30 min. For the cell without the catalyst, the charging voltage starts at 3.8 V and gradually increases to 4.7 V, the cutoff voltage (Figure 3e). The charging time is about 17 h, contributing to a Coulombic efficiency of 85%. Due to the gas phase change in the sodium−air battery, small voltage fluctuations are observed on the charging profile. As can be seen, the oxygen gas releases at the beginning of the charge and then reaches almost the theoretical two-electron transfer line, indicating a quasi-two-electron transfer reaction. At the end of the charge, the amount of O_2 decreases while CO_2 starts to release when the voltage goes up to 4.7 V. The voltage exceeds the voltage window of the ether solvent, so the solvent could decompose at such a high voltage, resulting in the CO_2 evolution. The cell with the PtNi/C catalyst displays a different trend of the gas evolution, shown in Figure 3f. The cell runs 20 h, leading to a 100% Coulombic efficiency, but CO_2 dominates the gas evolution at the end of the charge. Under a charging voltage of 2.8 V, O_2 is generated close to the theoretical line almost the whole time of the charge, which is different from the cell without the catalyst. The larger amount of O_2 evolution suggests a better reversibility when PtNi/C catalyst is applied in the cell. Based on the findings, we propose the reaction in the sodium−air battery is $2Na + O_2 + 2H_2O \leftrightarrow Na_2O_2·2H_2O$.

The post mortem analysis was conducted in a Na−air battery with the PtNi catalyst after 100 cycles. For the cathode, we do not observe much products left on the catalyst side facing the separator (Figure S8a) nor the side exposed to the air (Figure S8b). In Raman measurements, we observe that signals are mainly from NaOH at 3638 cm^{-1} and Na_2CO_3 at 1078 cm^{-1}, indicating the accumulation of side products on the air electrode during 100 cycles, as shown in Figure S8c. However, even after 100 cycles, the cathode still maintains its structure and does not suffer a pore-clogging issue, which indicates that the cathode is probably not the reason for the cell failure.

On the other hand, the sodium metal anode does not suffer severe decomposition when the cell is exposed to air within 10 cycles. A dense SEI layer was formed on the surface of Na (Figure 4a). XRD of the cycled anode (Figure 4b) shows that NaOH is the major component on the surface besides the sodium metal after 10 cycles in air. Nevertheless, the anode also suffers decomposition during a long cycling test after 100 cycles. Figure S9 shows the optical images of the Na anode after 100 cycles. The side facing the separator (Figure S9a) loses all of the metallic luster and becomes white, indicating the decay of the Na metal and the formation of the side products. On the other side of the Na anode (facing the current collector, Figure S9b), only a small portion of Na metal is left. The white piece of the anode was cut and further characterized by Raman and XRD. In Figure 4c, Raman shows sharp peaks of Na_2CO_3 at 1078 cm^{-1} and NaOH at 3638 cm^{-1}. We also observe the two side products in XRD, shown in

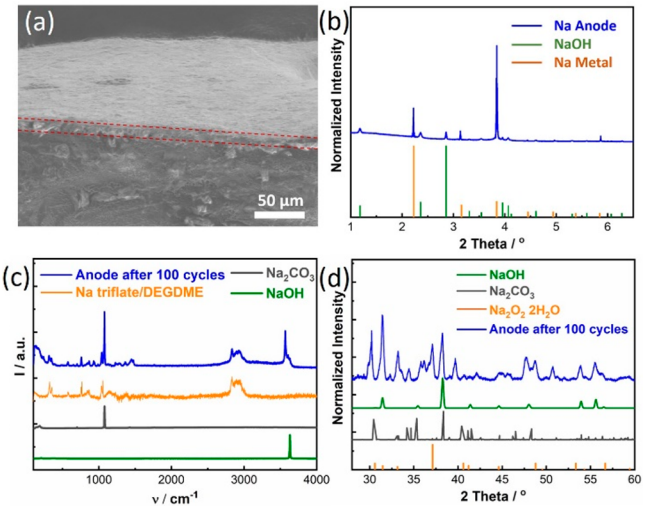

Figure 4. (a) SEM and (b) XRD of the sodium anode after 10 cycles in a Na−air battery. (c) Raman and (d) XRD of the sodium anode after 100 cycles in a Na−air battery.

Figure 4d. Additionally, it is very likely to have $Na_2O_2·2H_2O$ on the anode. Currently, we could not assign all of the minor peaks in XRD, but the result shows that the anode experiences more parasitic reactions than does the cathode. Interestingly, although a thick layer of side products grows on the surface of the anode, it does not prevent the Na^+ transport, and the cell could still run over 100 cycles. Nevertheless, the Na metal would be subsequently depleted and lead to the death of the cell. Hence, we propose that the depletion of the anode is very likely the reason for the cell failure.

The depletion of Na is a severe issue not only for Na−air batteries but also for Na−O_2 batteries. However, more oxidative products were observed in the Na anode in an O_2-rich environment such as NaO_2 and Na_2O_2,[26] originating from the effect of oxygen crossover. We compared the cycling efficiency of the Na anodes in Na−O_2 and Na−air batteries, shown in Figure S10, where the Na anode in air has a cycling efficiency higher than that in O_2. Our results show that replacing O_2 with air is beneficial to the sodium anode because the concentration of O_2 has been largely reduced from 100 to ∼20%, indicating the suppression of oxygen crossover. In addition, different from Li metal, which reacts with N_2 to form Li_3N, N_2 is inert to Na metal. More importantly, the small amount of water in air or in the electrolyte could lead to the formation of NaOH on the anode as a protecting layer. On the other hand, we did not observe the dendrite formation of the sodium metal in the air cell, which is different from the scenario in the oxygen cell (Figure S11). In sodium−oxygen batteries, sodium dendrite formation is always a safety concern that could short circuit the cell after a few cycles.[26,40,41] While in the air atmosphere, the cycle life of the cell runs over 100 cycles, indicating that dendrite penetration does not occur. The composition of the SEI layer requires detailed investigation to evaluate the stability of the sodium anode in the future.

CONCLUSIONS

In conclusion, we successfully achieve a secondary sodium−air battery which is able to cycle in air atmosphere with decent stability and long cycle life. Without an oxygen evolution reaction catalyst, the sodium−air batteries have a cycle life of

https://dx.doi.org/10.1021/acs.nanolett.0c01670
Nano Lett. 2020, 20, 4681−4686

80 cycles; after an alloy catalyst was applied, the charge potential decreased from over 4.0 V to below 2.7 V, leading to a much-improved energy efficiency. The cyclability has been improved to over 100 cycles. The cells are cycled based on the reversible formation/decomposition of the discharge product, $Na_2O_2{\cdot}2H_2O$. This type of sodium−air battery is a big step toward real applications in the field of energy storage.

■ ASSOCIATED CONTENT

Supporting Information

The Supporting Information is available free of charge at https://pubs.acs.org/doi/10.1021/acs.nanolett.0c01670.

Experimental, characterization, and additional results (PDF)

■ AUTHOR INFORMATION

Corresponding Authors

Jun Lu − *Chemical Sciences and Engineering Division, Argonne National Laboratory, Lemont, Illinois 60439, United States;* orcid.org/0000-0003-0858-8577; Email: junlu@anl.gov

Khalil Amine − *Chemical Sciences and Engineering Division, Argonne National Laboratory, Lemont, Illinois 60439, United States; Department of Material Science and Engineering, Stanford University, Stanford, California 94305, United States;* orcid.org/0000-0001-9206-3719; Email: amine@anl.gov

Authors

Xuanxuan Bi − *Chemical Sciences and Engineering Division, Argonne National Laboratory, Lemont, Illinois 60439, United States;* orcid.org/0000-0003-4910-7194

Rongyue Wang − *Applied Materials Division, Argonne National Laboratory, Lemont, Illinois 60439, United States*

Yifei Yuan − *Chemical Sciences and Engineering Division, Argonne National Laboratory, Lemont, Illinois 60439, United States; Department of Mechanical and Industrial Engineering, University of Illinois at Chicago, Chicago, Illinois 60607, United States*

Dongzhou Zhang − *HIGP, University of Hawaii at Manoa, Honolulu, Hawaii 96822, United States*

Tao Zhang − *Material Sciences Division, Argonne National Laboratory, Lemont, Illinois 60439, United States*

Lu Ma − *X-ray Science Division, Argonne National Laboratory, Lemont, Illinois 60439, United States*

Tianpin Wu − *X-ray Science Division, Argonne National Laboratory, Lemont, Illinois 60439, United States*

Reza Shahbazian-Yassar − *Department of Mechanical and Industrial Engineering, University of Illinois at Chicago, Chicago, Illinois 60607, United States;* orcid.org/0000-0002-7744-4780

Complete contact information is available at: https://pubs.acs.org/10.1021/acs.nanolett.0c01670

Notes

The authors declare no competing financial interest.

■ ACKNOWLEDGMENTS

This work is supported by the U.S. Department of Energy (DOE), Office of Energy Efficiency and Renewable Energy, Vehicle Technologies Office. Argonne National Laboratory is operated for DOE Office of Science by UChicago Argonne, LLC, under contract number DE-AC02-06CH11357. Use of the Center for Nanoscale Materials, an Office of Science user facility, and use of the Advanced Photon Source (9-BM) were supported by the U.S. Department of Energy, Office of Basic Energy Sciences under Contract No. DE-AC02-06CH11357. 13BM-C operation was supported by COMPRES through the Partnership for Extreme Crystallography (PX^2) project, under the NSF Cooperative Agreement EAR 11-57758. R.S.-Y. acknowledges the NSF-DMR Award No. 1620901.

■ REFERENCES

(1) Lu, J.; Li, L.; Park, J. B.; Sun, Y. K.; Wu, F.; Amine, K. Aprotic and aqueous Li-O(2) batteries. *Chem. Rev.* **2014**, *114* (11), 5611−40.

(2) Geng, D.; Ding, N.; Hor, T. S. A.; Chien, S. W.; Liu, Z.; Wuu, D.; Sun, X.; Zong, Y. From Lithium-Oxygen to Lithium-Air Batteries: Challenges and Opportunities. *Adv. Energy Mater.* **2016**, *6* (9), 1502164.

(3) Liu, D.; Tong, Y.; Yan, X.; Liang, J.; Dou, S. X. Recent Advances in Carbon-Based Bifunctional Oxygen Catalysts for Zinc-Air Batteries. *Batteries & Supercaps* **2019**, *2*, 743.

(4) Feng, N.; He, P.; Zhou, H. Critical Challenges in Rechargeable Aprotic Li-O_2 Batteries. *Adv. Energy Mater.* **2016**, *6* (9), 1502303.

(5) Lin, X.; Sun, Q.; Doyle Davis, K.; Li, R.; Sun, X. The application of carbon materials in nonaqueous Na-O_2 batteries. *Carbon Energy* **2019**, *1*, 141.

(6) Zhang, X.; Chen, A.; Jiao, M.; Xie, Z.; Zhou, Z. Understanding Rechargeable Li-O_2 Batteries via First-Principles Computations. *Batteries & Supercaps* **2019**, *2*, 498.

(7) Aurbach, D.; McCloskey, B. D.; Nazar, L. F.; Bruce, P. G. Advances in understanding mechanisms underpinning lithium−air batteries. *Nat. Energy* **2016**, *1* (9), 16128.

(8) Shao, Y.; Ding, F.; Xiao, J.; Zhang, J.; Xu, W.; Park, S.; Zhang, J.-G.; Wang, Y.; Liu, J. Making Li-Air Batteries Rechargeable: Material Challenges. *Adv. Funct. Mater.* **2013**, *23* (8), 987−1004.

(9) Hong, Y.-S.; Zhao, C.-Z.; Xiao, Y.; Xu, R.; Xu, J.-J.; Huang, J.-Q.; Zhang, Q.; Yu, X.; Li, H. Safe Lithium-Metal Anodes for Li-O_2 Batteries: From Fundamental Chemistry to Advanced Characterization and Effective Protection. *Batteries & Supercaps* **2019**, *2*, 638.

(10) Zhao, W.; Mu, X.; He, P.; Zhou, H. Advances and Challenges for Aprotic Lithium-Oxygen Batteries using Redox Mediators. *Batteries & Supercaps* **2019**, *2*, 803.

(11) Landa-Medrano, I.; Pinedo, R.; Bi, X.; Ruiz de Larramendi, I.; Lezama, L.; Janek, J.; Amine, K.; Lu, J.; Rojo, T. New Insights into the Instability of Discharge Products in Na-O_2 Batteries. *ACS Appl. Mater. Interfaces* **2016**, *8* (31), 20120−7.

(12) Sun, B.; Pompe, C.; Dongmo, S.; Zhang, J.; Kretschmer, K.; Schröder, D.; Janek, J.; Wang, G. Challenges for Developing Rechargeable Room-Temperature Sodium Oxygen Batteries. *Adv. Mater. Technol.* **2018**, *3* (9), 1800110.

(13) Xu, S.; Wei, S.; Wang, H.; Abruna, H. D.; Archer, L. A. The Sodium-Oxygen/Carbon Dioxide Electrochemical Cell. *ChemSusChem* **2016**, *9* (13), 1600−6.

(14) Pinedo, R.; Weber, D. A.; Bergner, B.; Schröder, D.; Adelhelm, P.; Janek, J. Insights into the Chemical Nature and Formation Mechanisms of Discharge Products in Na−O_2 Batteries by Means of Operando X-ray Diffraction. *J. Phys. Chem. C* **2016**, *120* (16), 8472−8481.

(15) Zhao, S.; Qin, B.; Chan, K.-Y.; Li, C.-Y. V.; Li, F. Recent Development of Aprotic Na-O_2 Batteries. *Batteries & Supercaps* **2019**, *2*, 725.

(16) Stephanou, S. E.; Seyb, E. J., Jr.; Kleinberg, J.; Shakely, R. H.; Schechter, W. H. SODIUM SUPEROXIDE. *Inorg. Synth.* **2007**, *4*, 82−85.

(17) Gilles, P. W.; Margrave, J. L. The Heats of Formation of Na_2O_2, NaO_2 and KO_2. *J. Phys. Chem.* **1956**, *60* (9), 1333−1335.

(18) Mekonnen, Y. S.; Christensen, R.; Garcia-Lastra, J. M.; Vegge, T. Thermodynamic and Kinetic Limitations for Peroxide and Superoxide Formation in Na-O_2 Batteries. *J. Phys. Chem. Lett.* **2018**, *9* (15), 4413−4419.

(19) Liu, C.; Carboni, M.; Brant, W. R.; Pan, R.; Hedman, J.; Zhu, J.; Gustafsson, T.; Younesi, R. On the Stability of NaO_2 in Na-O_2 Batteries. *ACS Appl. Mater. Interfaces* **2018**, *10* (16), 13534−13541.
(20) Lin, X.; Sun, Q.; Yadegari, H.; Yang, X.; Zhao, Y.; Wang, C.; Liang, J.; Koo, A.; Li, R.; Sun, X. On the Cycling Performance of Na-O_2 Cells: Revealing the Impact of the Superoxide Crossover toward the Metallic Na Electrode. *Adv. Funct. Mater.* **2018**, *28* (35), 1801904.
(21) Asadi, M.; Sayahpour, B.; Abbasi, P.; Ngo, A. T.; Karis, K.; Jokisaari, J. R.; Liu, C.; Narayanan, B.; Gerard, M.; Yasaei, P.; Hu, X.; Mukherjee, A.; Lau, K. C.; Assary, R. S.; Khalili-Araghi, F.; Klie, R. F.; Curtiss, L. A.; Salehi-Khojin, A. A lithium-oxygen battery with a long cycle life in an air-like atmosphere. *Nature* **2018**, *555* (7697), 502−506.
(22) Sun, Q.; Yadegari, H.; Banis, M. N.; Liu, J.; Xiao, B.; Li, X.; Langford, C.; Li, R.; Sun, X. Toward a Sodium−"Air" Battery: Revealing the Critical Role of Humidity. *J. Phys. Chem. C* **2015**, *119* (24), 13433−13441.
(23) Yadegari, H.; Sun, X. Recent Advances on Sodium-Oxygen Batteries: A Chemical Perspective. *Acc. Chem. Res.* **2018**, *51* (6), 1532−1540.
(24) Bi, X.; Wang, R.; Ma, L.; Zhang, D.; Amine, K.; Lu, J. Sodium Peroxide Dihydrate or Sodium Superoxide: The Importance of the Cell Configuration for Sodium-Oxygen Batteries. *Small Methods* **2017**, *1* (7), 1700102.
(25) Kim, J.; Park, H.; Lee, B.; Seong, W. M.; Lim, H. D.; Bae, Y.; Kim, H.; Kim, W. K.; Ryu, K. H.; Kang, K. Dissolution and ionization of sodium superoxide in sodium-oxygen batteries. *Nat. Commun.* **2016**, *7*, 10670.
(26) Bi, X.; Ren, X.; Huang, Z.; Yu, M.; Kreidler, E.; Wu, Y. Investigating dendrites and side reactions in sodium-oxygen batteries for improved cycle lives. *Chem. Commun. (Cambridge, U. K.)* **2015**, *51* (36), 7665−8.
(27) Assary, R. S.; Lu, J.; Du, P.; Luo, X.; Zhang, X.; Ren, Y.; Curtiss, L. A.; Amine, K. The effect of oxygen crossover on the anode of a Li-O(2) battery using an ether-based solvent: insights from experimental and computational studies. *ChemSusChem* **2013**, *6* (1), 51−5.
(28) Yuan, Y.; Lu, J. Demanding energy from carbon. *Carbon Energy* **2019**, *1*, 8.
(29) Wang, H.; Cui, Y. Nanodiamonds for energy. *Carbon Energy* **2019**, *1*, 13.
(30) Or, T.; Gourley, S. W. D.; Kaliyappan, K.; Yu, A.; Chen, Z. Recycling of mixed cathode lithium-ion batteries for electric vehicles: Current status and future outlook. *Carbon Energy* **2020**, *2*, 6.
(31) Paul, R.; Dai, Q.; Hu, C.; Dai, L. Ten years of carbon-based metal-free electrocatalysts. *Carbon Energy* **2019**, *1*, 19.
(32) Bender, C. L.; Schroder, D.; Pinedo, R.; Adelhelm, P.; Janek, J. One- or Two-Electron Transfer? The Ambiguous Nature of the Discharge Products in Sodium-Oxygen Batteries. *Angew. Chem., Int. Ed.* **2016**, *55* (15), 4640−9.
(33) Brame, E. G., Jr.; Cohen, S.; Margrave, J. L.; Meloche, V. W. INFRA-RED SPECTRA OF INORGANIC SOLIDS-I PEROXIDES, PEROXIDE HYDRATES, AND SUPEROXIDES. *J. Inorg. Nucl. Chem.* **1957**, *4*, 90−92.
(34) Yadegari, H.; Li, Y.; Banis, M. N.; Li, X.; Wang, B.; Sun, Q.; Li, R.; Sham, T.-K.; Cui, X.; Sun, X. On rechargeability and reaction kinetics of sodium−air batteries. *Energy Environ. Sci.* **2014**, *7* (11), 3747−3757.
(35) Hartmann, P.; Bender, C. L.; Vracar, M.; Durr, A. K.; Garsuch, A.; Janek, J.; Adelhelm, P. A rechargeable room-temperature sodium superoxide (NaO2) battery. *Nat. Mater.* **2013**, *12* (3), 228−32.
(36) Nawwar, M.; Poon, R.; Chen, R.; Sahu, R. P.; Puri, I. K.; Zhitomirsky, I. High areal capacitance of Fe3O4-decorated carbon nanotubes for supercapacitor electrodes. *Carbon Energy* **2019**, *1*, 124.
(37) Shi, Y.; Liu, G.; Jin, R.; Xu, H.; Wang, Q.; Gao, S. Carbon materials from melamine sponges for supercapacitors and lithium battery electrode materials: A review. *Carbon Energy* **2019**, *1*, 253.
(38) Yuan, Y.; Amine, K.; Lu, J.; Shahbazian-Yassar, R. Understanding materials challenges for rechargeable ion batteries with in situ transmission electron microscopy. *Nat. Commun.* **2017**, *8* (1), 15806.
(39) Wang, C.; Chi, M.; Li, D.; Strmcnik, D.; van der Vliet, D.; Wang, G.; Komanicky, V.; Chang, K. C.; Paulikas, A. P.; Tripkovic, D.; Pearson, J.; More, K. L.; Markovic, N. M.; Stamenkovic, V. R. Design and synthesis of bimetallic electrocatalyst with multilayered Pt-skin surfaces. *J. Am. Chem. Soc.* **2011**, *133* (36), 14396−403.
(40) Yang, H.; Sun, J.; Wang, H.; Liang, J.; Li, H. A titanium dioxide nanoparticle sandwiched separator for Na-O2 batteries with suppressed dendrites and extended cycle life. *Chem. Commun. (Cambridge, U. K.)* **2018**, *54* (32), 4057−4060.
(41) Wu, S.; Qiao, Y.; Jiang, K.; He, Y.; Guo, S.; Zhou, H. Tailoring Sodium Anodes for Stable Sodium-Oxygen Batteries. *Adv. Funct. Mater.* **2018**, *28* (13), 1706374.

https://dx.doi.org/10.1021/acs.nanolett.0c01670
Nano Lett. 2020, 20, 4681−4686